Simulating Incompressible Fluid Flow in a Channel: From Poiseuille's Law to Realistic Navier-Stokes Solutions

0. Abstract

This study uses numerical simulations to investigate incompressible fluid flow in a channel, beginning with the ideal laminar case described by Poiseuille's law and extending to more realistic conditions. A full 2D Navier–Stokes solver was implemented to explore the effects of channel constrictions, wall roughness, and varying Reynolds numbers. The simulations reproduce the classical parabolic velocity profile in smooth channels and reveal how constrictions generate jet-like acceleration, recirculation zones, and vortex shedding. Quantitative analysis shows that flow resistance and energy dissipation rise with both Reynolds number and constriction severity, while sharp step-like constrictions amplify vortex shedding compared to smooth Gaussian ones. Particle transport was also modeled, highlighting inertial focusing on low Reynolds numbers and increased wall deposition at higher Reynolds numbers, especially near constrictions. These results illustrate how channel imperfections and flow instabilities contribute to energy losses and particle accumulation, with implications for understanding vascular blockages and pipeline fouling. Although limited to two dimensions and moderate simulation times, the work demonstrates the power of the Navier–Stokes framework in capturing complex flow behavior and points toward future three-dimensional studies with potential applications in engineering and medicine.

Keywords: Fluid dynamics, Navier-Stokes equations, rectangular channel, Reynolds number, laminar flow, turbulence, vortex shedding, sedimentation

1. Introduction

Fluid dynamics governs how liquids and gases move, from phenomena like water flow in channels, air around airplane wings to ocean currents. The mathematical models to describe the motion of viscous fluid substances were developed in the 19th century as the Navier-Stokes equations, by applying Newton's second law to fluid, accounting for viscosity, pressure, and external forces[2,3]. They are a set of partial differential equations (PDE), however, are notoriously difficult to solve analytically due to their nonlinear and coupled nature. The nonlinear convective term in the equation causes chaotic behavior, i.e. the solution is highly sensitive to initial conditions. The velocity and pressure fields are interdependent, making the system a set of coupled PDEs. In 2000, the Clay Mathematics Institute designated the Navier-Stokes existence and smoothness problem as one of its seven Millennium Prize Problems[1].

While the general analytical solutions to Navier-Stokes equations are still elusive and probably non-existing in 3D, there are a few simple cases with existing analytical solutions by some assumptions of steady-state, incompressibility, and certain symmetry to simplify the equations[4]. Laminar flow is one of the simplest types of fluid motion. It occurs when a fluid flows in parallel

layers, with minimal mixing and no turbulence. The velocity field in the steady state is described by Poiseuille's law[5]. Real-world pipes, however, like blood vessels or industrial pipelines, have imperfections such as constrictions and rough surfaces. Flows may become unsteady or turbulent and result in large pressure drops along the channels and energy losses.

This study investigated fluid flow in a channel by starting with Poiseuille's Law and progressively adding complexity to approach realistic scenarios. Using numerical simulations by a full 2D Navier-Stokes solution without the laminar assumption, I modeled: (1) laminar flow in an ideal smooth no-slip channel that a parabolic velocity profile is developed in the channel regardless of Re numbers (2) turbulence and vortex shedding which deviate from laminar flow with different shapes of constrictions and random roughness (3) particle transport and deposition in the flow to study clogging at constrictions under varying Re numbers. The research is to understand: How channel imperfections and unsteady effects can alter flow compared to the ideal Poiseuille case, and how these changes contribute to energy losses, and reveal about the Navier-Stokes equations' complexity. The combined analytical and numerical methods explore ideal and realistic flow scenarios, offering insights into engineering (e.g., pipeline design) and medical applications (e.g., blood flow in arteries).

1.1. Navier-Stokes Equations

I start by introducing the Navier-Stokes equations for an incompressible fluid:
Momentum Equation:

$$\frac{\partial u}{\partial t} + (u \cdot \nabla)u = -\frac{1}{\rho}\nabla p + \nu\nabla^2 u + G$$

Continuity Equation:

$$\nabla \cdot u = 0$$

Here:

- $u = (u_x, u_y, u_z)$: Velocity vector field of the fluid.
- t: Time.
- ρ: Density of fluid.
- p: Pressure field.
- ν: Viscosity of fluid.
- G: External forces.
- ∇: Gradient operator.
- ∇^2: Laplacian operator.
- $(u \cdot \nabla)u$: Convective term.

The equations describe how the velocity, pressure and density of a fluid evolve over time and space. It is instructive to understand each term in the momentum equation: $\frac{\partial u}{\partial t}$ is the rate of change of the velocity field or acceleration of fluid particles; $(u \cdot \nabla)u$ is the nonlinear convective term, representing how the fluid's velocity transports itself, leading to complex behaviors like turbulence;

$-\frac{1}{\rho}\nabla p$ is the pressure gradient force, driving fluid from high to low pressure; $\nu\nabla^2 u$ is the viscous term, modeling the diffusion of momentum due to viscosity; G is external forces, such as gravity or electromagnetic forces. The continuity equation ensures mass conservation, i.e. for an incompressible fluid, the volume of fluid entering a region equals the volume leaving it[4].

1.2. Poiseuille's Law

Poiseuille's Law is a specific solution to Navier-Stokes equations under simplified conditions for laminar flow in a cylindrical channel[5]. The laminar flow is in steady state and moving in parallel layers, so $\frac{\partial u}{\partial t} = 0$ and $(u \cdot \nabla)u = 0$. The velocity field in a cylindrical channel does not change along the channel's length, only varying radially, therefore, in a cylindrical coordinate (r, θ, z), the velocity field $u = (u_r, u_\theta, u_z) = (u_r, 0, 0)$, where r is the radial distance from the channel center, θ is the angular corrdinate, z is the axial direction along the channel. Pressure only varies along z with a constant pressure gradient $\frac{\partial p}{\partial z} = -\frac{\Delta P}{L}$ and there are no external forces along the channel.

The Navier-Stokes equation in the z-direction becomes:

$$0 = \frac{\Delta P}{L} + \mu\left(\frac{1}{r}\frac{\partial}{\partial r}\left(r\frac{\partial u}{\partial r}\right)\right)$$

Rearrange the equation:

$$\frac{\partial}{\partial r}\left(r\frac{\partial u}{\partial r}\right) = -\frac{\Delta P}{\mu L}r$$

Integrate with respect to r:

$$r\frac{\partial u}{\partial r} = -\frac{\Delta P}{2\mu L}r^2 + C_1$$

$$\frac{\partial u}{\partial r} = -\frac{\Delta P}{2\mu L}r + \frac{C_1}{r}$$

To avoid singularity at $r = 0$, set the constant $C_1 = 0$:

$$\frac{\partial u}{\partial r} = -\frac{\Delta P}{2\mu L}r$$

Integrate again:

$$u = -\frac{\Delta P}{4\mu L}r^2 + C_2$$

Apply the no-slip boundary condition $u(R) = 0$ at the channel wall:

$$0 = -\frac{\Delta P}{4\mu L}R^2 + C_2$$

I obtain the parabolic velocity profile for laminar flow in a channel:

$$u(r) = \frac{\Delta P}{4\mu L}(R^2 - r^2)$$

The Poiseuille's Law describes the relationship between volume flow rate and pressure drop of laminar flow through a long cylindrical channel and is therefore obtained by integrating the above equation over the channel's cross-sectional area:

$$\begin{aligned} Q &= \int_0^R u\,(r) \cdot 2\pi r dr \\ &= \int_0^R \frac{\Delta P}{4\mu L}(R^2 - r^2) \cdot 2\pi r dr \\ &= \frac{\pi \Delta P R^4}{8\mu L} \end{aligned}$$

1.3. Full 2D Navier-Stokes Simulation

Analytical solution to the Navier-Stokes equations is difficult, however, the numerical methods and approximations allow engineers and scientists to use the Navier-Stokes equations effectively to study fluid dynamics in complex geometries as in aerodynamics and weather modeling. Without going to the full extent to simulate the fluid flow in 3D, which might require commercial software and significant computational power, I solve the incompressible Navier-Stokes equations in a 2D rectangular channel, which represents a cut-away view of a pipeline, with different shapes of constrictions and random wall roughness, to capture time-dependent and turbulence-like effects.
The incompressible Navier-Stokes equations in 2D are:
Momentum equation:

$$\frac{\partial u_x}{\partial t} + u_x \frac{\partial u_x}{\partial x} + u_y \frac{\partial u_x}{\partial y} = -\frac{1}{\rho}\frac{\partial p}{\partial x} + \nu\left(\frac{\partial^2 u_x}{\partial x^2} + \frac{\partial^2 u_x}{\partial y^2}\right) + G$$

$$\frac{\partial u_y}{\partial t} + u_x \frac{\partial u_y}{\partial x} + u_y \frac{\partial u_y}{\partial y} = -\frac{1}{\rho}\frac{\partial p}{\partial y} + \nu\left(\frac{\partial^2 u_y}{\partial x^2} + \frac{\partial^2 u_y}{\partial y^2}\right) + G$$

Continuity equation:

$$\frac{\partial u_x}{\partial x} + \frac{\partial u_y}{\partial y} = 0$$

The external body force $G = (G, 0)$ is applied in the x-direction and serves as the driving force to induce and sustain the fluid flow through the channel, which is equivalent to a constant pressure gradient and central to Poiseuille's Law. This is a common numerical technique in computational fluid dynamics (CFD) simulations of channel or Poiseuille-like flows. If without non-zero G in simulation and the simulation starts from rest, $u_x = u_y = 0$, the velocities will remain zero indefinitely, as there's nothing to initiate motion and the flow would be stagnant with no time evolution.

In the early 20th century, the Stream Function–Vorticity formulation emerged, e.g. in Horace Lamb's Hydrodynamics 1879, as an alternative way to write the Navier–Stokes equations. It is particularly useful for 2D incompressible flows. It simplifies the equations by eliminating the

pressure term by working with vorticity (ω) and automatically satisfying continuity equation using a stream function (ψ).

The stream function is defined such that the continuity is satisfied automatically:

$$u_x = \frac{\partial \psi}{\partial y}, \qquad u_y = -\frac{\partial \psi}{\partial x}$$

Vorticity is the curl of the velocity field to measure rotation:

$$\omega = \frac{\partial u_y}{\partial x} - \frac{\partial u_x}{\partial y}$$

I can therefore plug in $u_x,\ u_y$ from stream function to get the Poisson equation connecting ω and ψ:

$$\begin{aligned} \omega &= \frac{\partial}{\partial x}\left(-\frac{\partial \psi}{\partial x}\right) - \frac{\partial}{\partial y}\left(\frac{\partial \psi}{\partial y}\right) \\ &= -\left(\frac{\partial^2 \psi}{\partial x^2} + \frac{\partial^2 \psi}{\partial y^2}\right) \\ &= -\nabla^2 \psi \end{aligned}$$

Take the curl of both sides of Navier-Stokes equation:

$$\nabla \times \left(\frac{\partial u}{\partial t} + (u \cdot \nabla)\mathrm{u}\right) = \nabla \times \left(-\frac{1}{\rho}\nabla \mathrm{p} + \nu \nabla^2 u + G\right)$$

Apply curl properties and obtain the vorticity transport equation:

$$\frac{\partial \omega}{\partial t} + (u \cdot \nabla)\omega = \nu \nabla^2 \omega$$

In 2D:

$$\frac{\partial \omega}{\partial t} + u_x \frac{\partial \omega}{\partial x} + u_y \frac{\partial \omega}{\partial y} = \nu \left(\frac{\partial^2 \omega}{\partial x^2} + \frac{\partial^2 \omega}{\partial y^2}\right)$$

In terms of physical meaning, vorticity represents the curl of the velocity field and quantifies the local angular velocity of fluid elements. It can reveal fine-scale structures that might be invisible in velocity field plot for detection of turbulent transitions. Streamlines are tangent to the velocity vector of the fluid and represent the paths a massless particle would flow.

1.4. Reynolds Number

The Reynolds number (Re) is a dimensionless quantity in fluid dynamics. It compares the relative importance of inertial forces to viscous forces in the fluid. It is defined as:

$$Re = \frac{\rho U L}{\mu} = \frac{UL}{\nu}$$

where ρ is the fluid density, U is a characteristic velocity (e.g., mean or maximum flow speed), L is a characteristic length scale (e.g., channel height or pipe diameter), μ is the dynamic viscosity, and ν is the kinematic viscosity. In the case of channel flow, Re is often computed using the

centerline velocity and half-channel height as $Re = \frac{GH^3}{16\nu^2}$ (where G is the driving force of the flow and H is the full channel height).

Physically, Re is used to characterize the nature of fluid flow: a) Laminar Flow: Typically occurs at low Re, $Re < 2{,}000$ for channel flow. The flow is smooth, with fluid moving in parallel layers where viscous forces dominate. b) Transitional Flow: Occurs at intermediate Re, e.g., $2{,}000 < Re < 4{,}000$, where the flow can change between laminar and turbulent. c) Turbulent Flow: Occurs at high Re, e.g., $Re > 5{,}000$. This is the region where inertial forces prevail, leading to chaotic, irregular motion and eddies in the flow[6].

It enables similarity analysis for results from models on different scales but similar Re number. This is essential in aerospace, automotive, and civil engineering for designing efficient systems without full-scale prototyping. Therefore, in my simulation Re is used as a control parameter to characterize different classes of flows from laminar to turbulent flow.

1.5. Flow with Channel Imperfections

I introduce channel imperfections to study how the laminar flow is affected by deviating from the ideal case. I add a constriction at the channel's midpoint which reduces the radius by up to 70% of the channel radius, mimicking the patient case of stenosis in coronary arteries with ≥ 70% narrowing often needing intervention of stent or bypass. The constriction shape can be either step-like, triangular or Gaussian with smooth narrowing. A random roughness of 1% of the radius is added to the channel wall. The combined effect of the constriction and wall roughness is to introduce irregular boundary conditions, therefore, contribute to the vortex or turbulence flow. The Poiseuille equation is used to compute velocity profiles and flow rates, comparing ideal and imperfect cases. The energy loss due to channel imperfections is calculated to be compared with ideal case.

1.6.Vortex shedding

In fluid dynamics, vortex shedding is created when a fluid flow past an obstacle at certain velocities. Periodic vortices are formed in the downstream, such as Von Kármán vortex street behind a cylinder. As a result, the periodic forces cause potential structural vibrations in engineering issues like bridge collapses or chimney swaying.

Mathematically, vortex shedding is characterized by the dimensionless Strouhal number (St), which relates the shedding frequency to flow parameters:

$$St = \frac{fD}{U}$$

where f is the shedding frequency, D is a characteristic length (e.g., constriction width or cylinder diameter), and U is the free-stream velocity (or mean channel velocity).

2. Results

2.1. Ideal Case

I start with the ideal case, i.e. the channel walls are smooth, no constrictions are present, and a constant external pressure gradient is applied to the flow along the channel direction. The simulation starts from rest at time zero and stops at 100 second. As a standard practice in CFD simulation, all quantities are calculated as dimensionless quantities to reduce the number of parameters and generalize findings applicable across different physical scales without dependency on specific units.

In Figure 1, it visualizes the simulation results at time 100s: the velocity magnitude $u = \sqrt{u_x^2 + u_y^2}$ and vorticity magnitude as color plots and streamline in the rectangular channel.

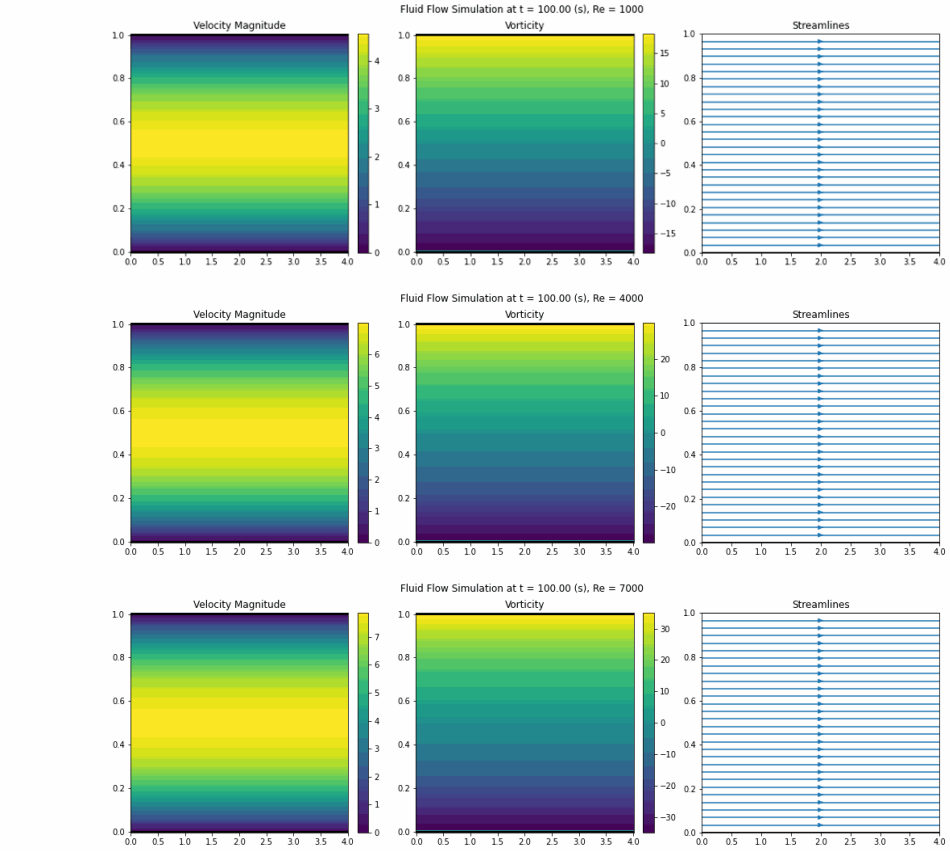

Figure 1: Velocity Field, Vorticity and Streamline of Fluid Flow at 100s in the Ideal Case with Different Re

The *Re* number is changing from 1,000 to 7,000. As can be observed, regardless of the *Re* number, the flows develop a similar profile with the highest velocity at the channel center and smoothly reduce to zero at the wall to satisfy the no-slip condition. The channel center velocity increases with higher *Re* number, as higher *Re* is indicating higher fluid velocity with all other factors remain constant. The vorticity and streamline plots demonstrate there is no curl of velocity field, and the fluid motion is characterized by smooth and orderly

movement of fluid particles in parallel layers, with no mixing between those layers. The observations are consistent with the Poiseuille's Law in the ideal case. Poiseuille's Law describes the ideal steady-state where the fluid's time evolution has reached its final state. In Figure 2, the simulated center velocity is plotted as a function of time for different Re number, and the dashed line is the theoretical Poiseuille's Law velocity as a comparison. It can be observed that the center velocity is approaching to the final Poiseuille's velocity in all cases but with different approaching rate. It takes longer time to reach the final steady state for fluid with higher Re number. This is because the time required for the initial velocity to propagate from the walls to the center is governed by the viscous diffusion timescale, which is approximately $t \sim L_y^2/\nu$, where L_y is the channel height and ν is the kinematic viscosity. At higher $Re \sim 1/\nu^2$, the viscosity ν is lower, this results in a longer diffusion time for higher Re.

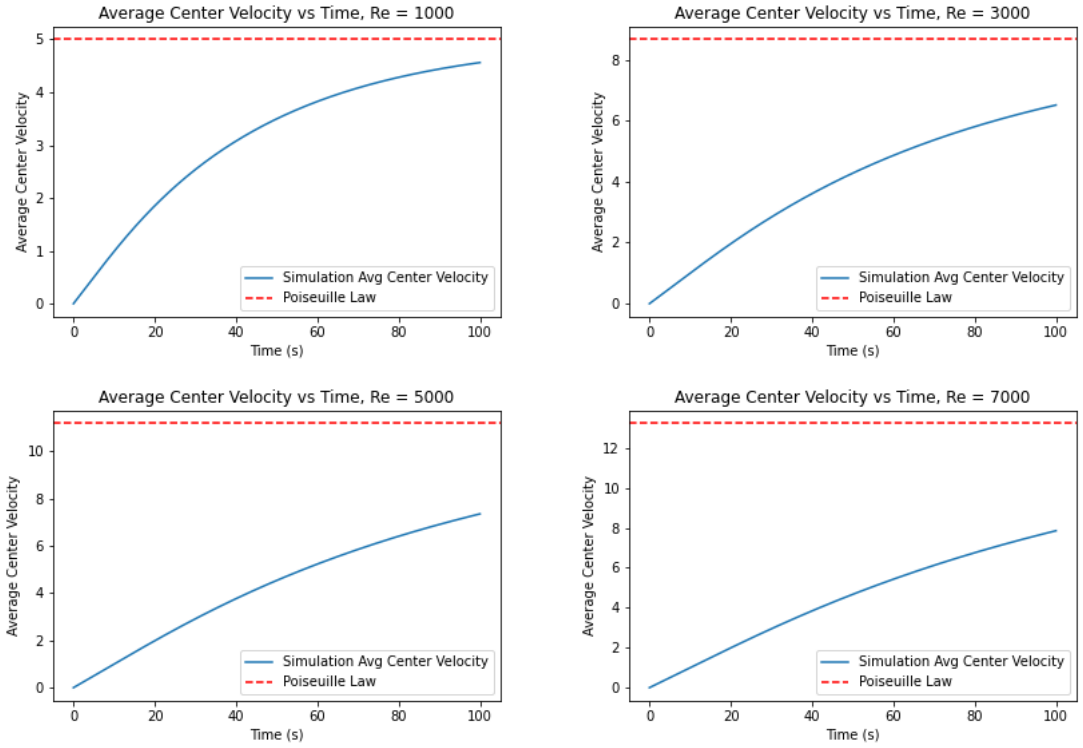

Figure 2: Channel Center Velocity as a Function of Simulation Time, Comparing with Poiseuille's Law

Therefore, approximately it is expected to see $t \sim L_y^2/\nu \sim L_y^2\sqrt{Re}$. For example, simulations show velocity reaches ~63% of steady state at 100 seconds at $Re = 7{,}000$ but it takes only ~40 seconds to reach the same velocity at $Re = 1{,}000$. Plug in the numbers from simulation, I observe the simulation matches with expectation consistently.

$$\frac{t_{Re=1,000}}{t_{Re=7,000}} = \frac{40}{100} \sim \frac{L_y^2\sqrt{1{,}000}}{L_y^2\sqrt{7{,}000}} \approx 0.38$$

2.2. Flow with perturbations

In the next study, I introduce perturbations, i.e. random roughness on the channel wall and different constriction shapes (Gaussian and step-like), to numerically investigate the system with hydraulic resistance, vortex shedding, and viscous energy dissipation in 2D channel flows, for *Re* ranging from 1,000 to 7,000. The wall roughness is kept as 1% of the channel radius and the constriction height increases from 5% to 35% of the channel radius to simulate different degree of constriction strength. The simulation results at 100s are shown in Figure 3 for Gaussian constriction at 5% strength. It is observed from the streamline plot that the overall flow remains laminar regardless of Re numbers, except that a variation of velocity at the center along the channel direction is induced by the constriction. A higher velocity, ~8%, is observed at the middle of constriction, compared to the leftmost inlet center far away from the middle of constriction. This is because of mass conservation (continuity equation), when the constriction reduces the cross-section area of the channel, the incompressible fluid passes through the narrower region with higher velocity. The vorticity plot shows some small curl of velocity field around the rough wall and constriction as expected.

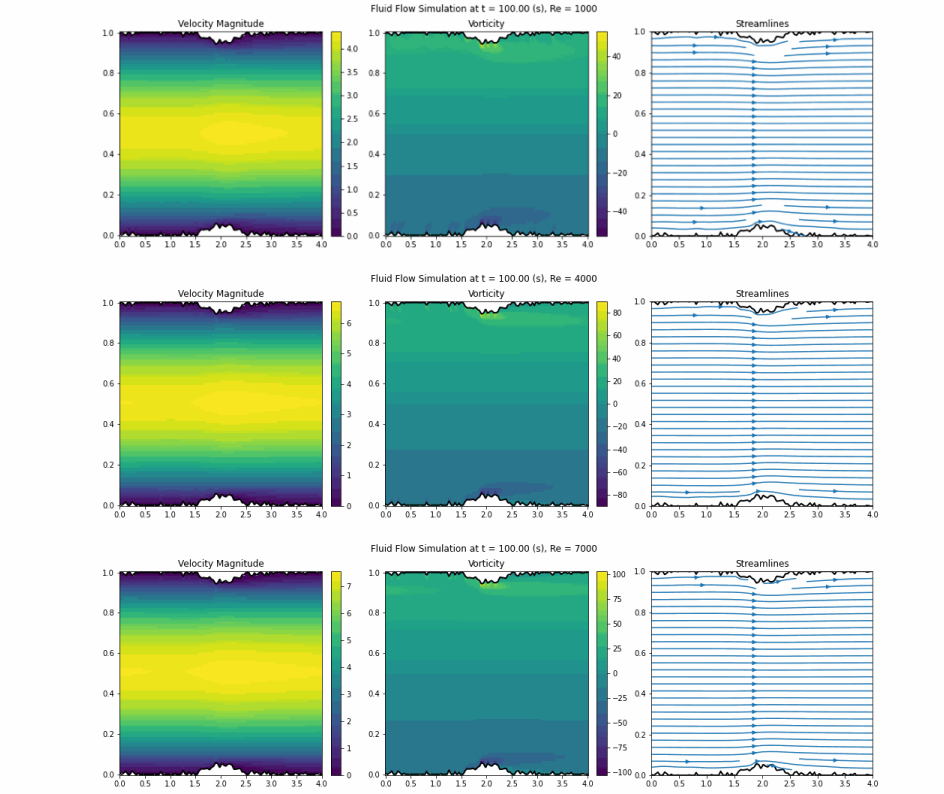

Figure 3: Fluid Flow at 100s with 5% Gaussian Constriction with Different Re

Now I turn to a more interesting case where the constriction strength is increased to 35% of the channel radius. As the simulation results become time dependent, two snapshots at 50s and 100s are shown in Figure 4. At 50s the flow accelerates significantly in the constriction region, indicating a jet-like flow through the narrowing. Alternating regions of positive and

negative vorticity suggest the formation of vortices. Streamlines converge smoothly into constriction with laminar entry condition. The upstream and downstream show clear recirculation zones due to constriction. At 100s, besides the pronounced high-speed jet flow through the constriction, the velocity and streamline plots show more evident curvature and instability, i.e. vortex shedding, but not fully turbulent with irregular eddies and no periodicity.

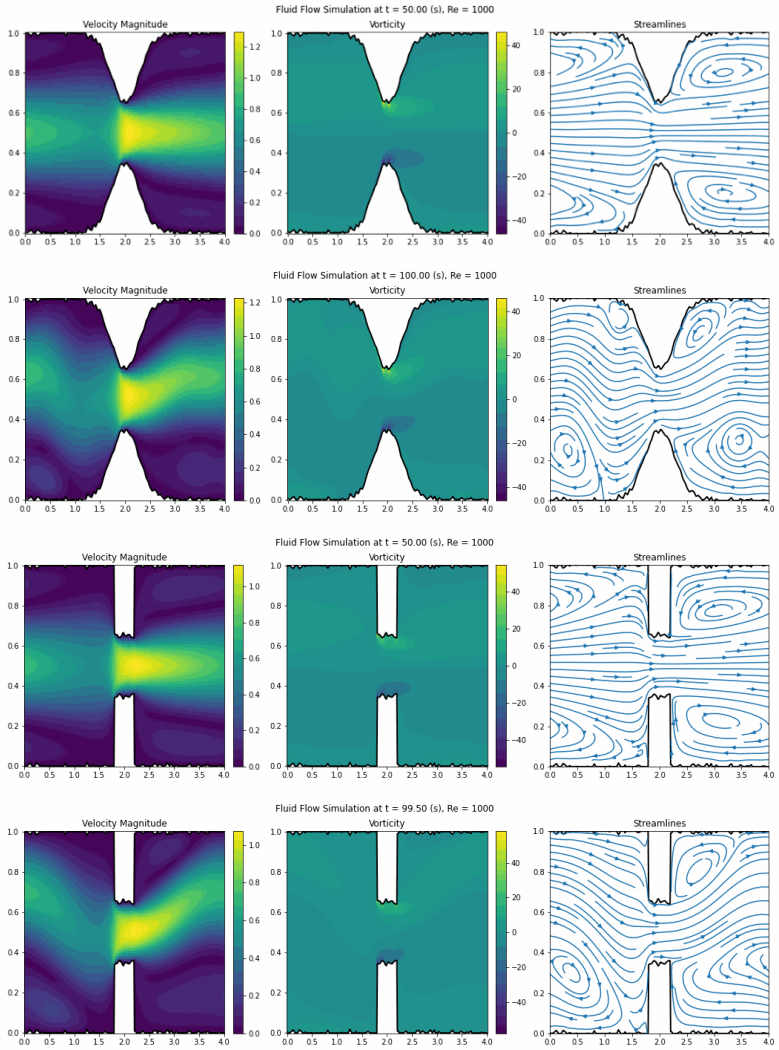

Figure 4: Fluid Flow with 35% Gaussian and Step Constriction at 50s and 100s with Re=1,000

If Re is raised to 7,000, significant inertial effect is introduced. As can be seen in Figure 5, periodic vortex shedding and unsteady flow starts to develop as early as 25s and become quasi-periodic at the simulation end time 100s. Compared to Re=1,000 case, stronger jets, larger vortices, and more significant recirculation can be observed. To quantify the observations for different simulation cases, I calculate three quantities: 1) Resistance R, defined as the pressure drop normalized by flow rate at the inlet $R = \Delta p/Q$. It measures the

hydraulic resistance. Higher R indicates greater difficulty for fluid to pass through, typically due to narrower sections, sharper geometries, or flow instabilities. 2) St, Strouhal number, as defined in Section 1.6, $St = fD/U$, f is the shedding frequency measured via FFT on the vorticity time series at a point downstream of the constriction, D is the width of constriction and U is the theoretical Poiseuille velocity at the center. 3) Diss, energy dissipation rate, as defined in Section 2.6. It measures the rate at which kinetic energy is converted to heat due to viscous friction.

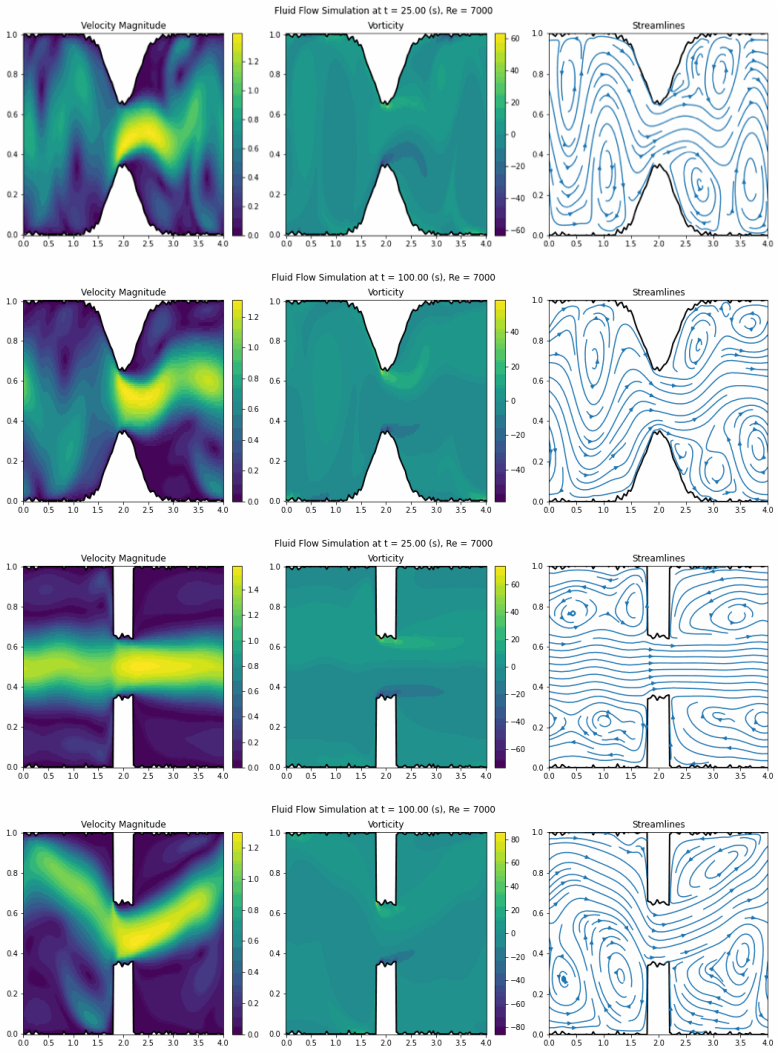

Figure 5: Fluid Flow with 35% Gaussian and Step Constriction at 25s and 100s with Re=7,000

The simulation results are summarized in Table 1 for constriction shape Gaussian and step-like, constriction strength is varied from 5% to 35% and Re is varied from 1,000 to 7,000. For both Gaussian and step shapes, R increases significantly with strength due to heightened flow obstruction, and generally rises with Re, reflecting inertial losses dominating at higher Re. Step shapes exhibit slightly higher R than Gaussian, because sharper geometries amplify

drag. St remains low overall (0.0002–0.0349) but shows spikes at high constriction strength/Re for Gaussian and step. Diss roughly remains flat at low constriction strength and Re for both shapes but increases with higher Re when constriction strength is high. This is reasonable because, at low constriction strength, the majority of the flow remains laminar regardless of Reynolds number, whereas at high constriction strength, the flow becomes unstable, developing more vortices and shedding, which increases energy dissipation[7,8].

Table 1: Constriction and Re Impact on Fluid Flow

Constriction Shape	Constriction Strength	Re	R	St	Diss
Gaussian	5%	1,000	0.84	0.0005	0.10
Gaussian	5%	4,000	2.93	0.0003	0.08
Gaussian	5%	7,000	4.43	0.0002	0.07
Gaussian	35%	1,000	5.32	0.0091	1.15
Gaussian	35%	4,000	16.30	0.0106	1.91
Gaussian	35%	7,000	30.53	0.0133	2.14
Step	5%	1,000	0.95	0.0005	0.08
Step	5%	4,000	3.69	0.0003	0.07
Step	5%	7,000	6.52	0.0009	0.07
Step	35%	1,000	5.76	0.0124	1.14
Step	35%	4,000	5.55	0.0152	1.06
Step	35%	7,000	5.96	0.0169	1.86

2.3. Particle Deposition in Channel Flow

The fluid flow simulations above reveal how constrictions and Re affect velocity profiles, vorticity, and energy dissipation, real-world applications such as blood flow in vessels or mass transport in pipelines often involve suspended particles that can deposit and cause blockages. To extend the analysis, I now incorporate particles into the channel flow and model their transport, sedimentation, and deposition under gravity, particularly at constrictions. This allows me to investigate clogging dynamics and how flow instabilities influence particle behavior.

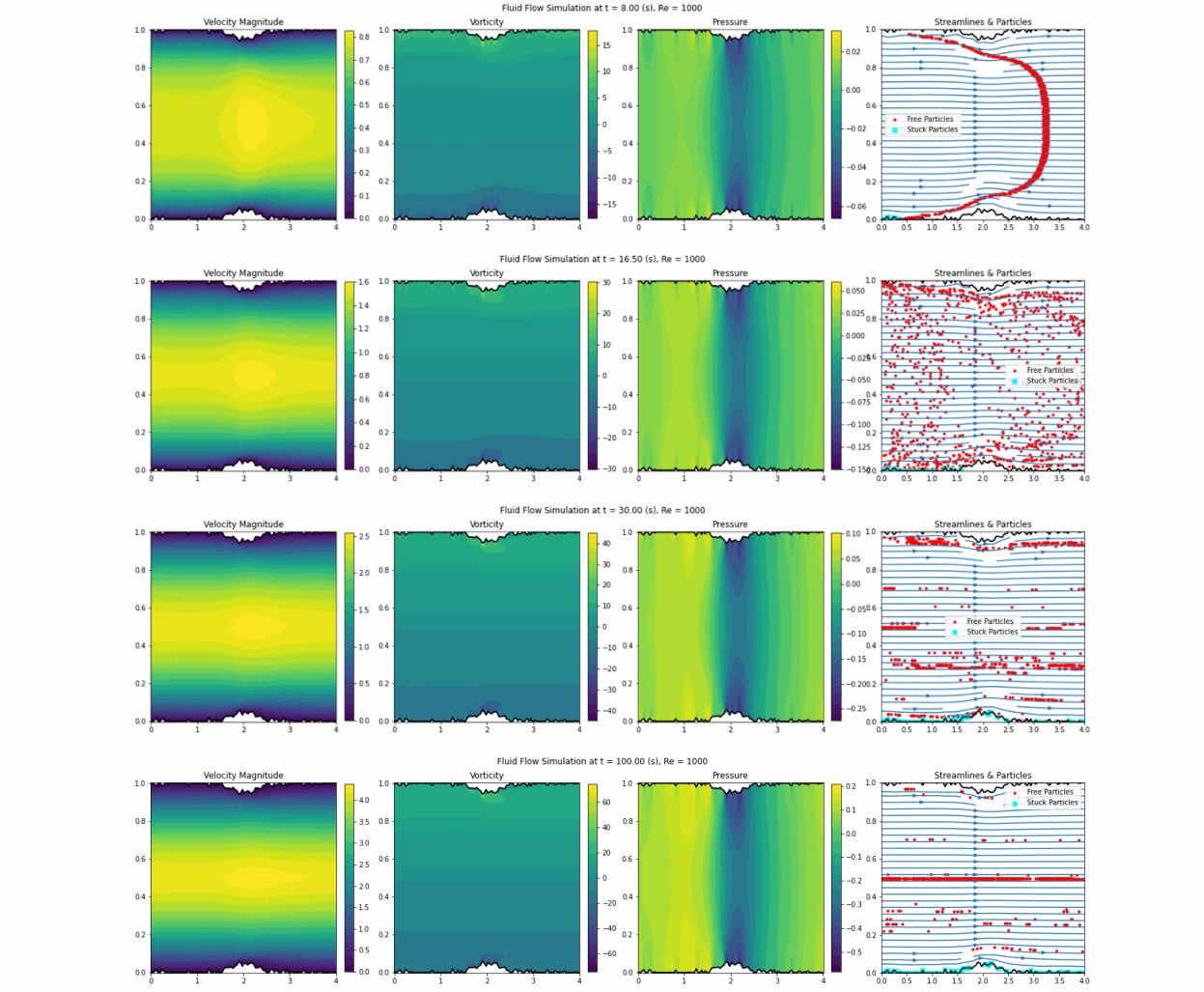

Figure 6: Particle Transport with Gaussian Constriction at 5% and Re of 1,000 at 8s, 16.5s, 30s and 100s

To simulate realistic scenarios, particles are added to the channel flow where each particle's motion is governed by Stokes drag from the fluid velocity, gravity-induced sedimentation, and probabilistic sticking upon wall collision (stick probability = 0.2)[9]. The simulation sweeps over Re = 1,000 and 7,000, constriction strengths = 5% and 35%, with 1,000 particles. I calculate the clog fraction as No. of stuck particles/total No. of particles. To simulate a continuous flow system, after the particles exits the channel at the right most outlet, they reenter the channel from the left inlet at random positions.

Figure 6 shows snapshots of particle positions and trajectories for Re = 1,000 and 5% strength. After 30s of simulation, it illustrates a phenomenon called inertial focusing, where particles align into streamlines near the channel center[10]. At moderate Re, inertial forces become significant compared to viscous forces. The nonlinear convective term in the Navier-Stokes equations causes particles to move away from the walls toward regions of lower shear, typically the channel center. often forming single-file lines or focused bands[11]. While at higher constriction strength of 35% in Figure 7, particles migrate toward walls, depositing near the constriction due to recirculation zones and gravity. At the end of simulation time, there is no inertial focusing that can carry particles through the flow, but significant number of particles deposited at the constriction.

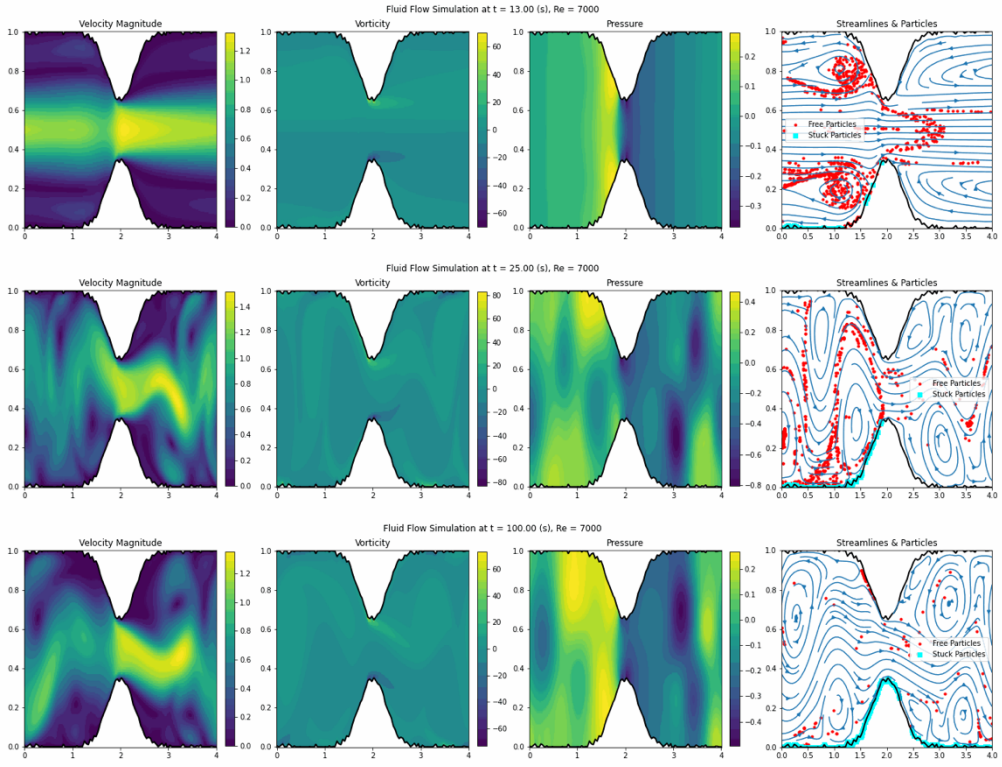

Figure 7: Particle Transport for Gaussian Constriction at 13s, 25s and 100s at Re=7,000

Figure 8 shows the accumulated particles density map at the end of simulation time. The clog fraction increases with Re and strength, from 0.45 at Re=1000, 5% to 0.92 at Re=7000, 35%. The higher inertia amplifies sedimentation and trapping. This aligns with studies on turbulent channel flows, where vortex shedding enhances deposition[12,13]. It effectively narrows the channel, mimicking arterial blockages or pipeline fouling. One limitation of the study is that it does not consider particle size effect and the probability of particle reentering into flow after deposition. These results still provide insights into the sedimentation or clog formation and help potential for optimizing designs to minimize deposition.

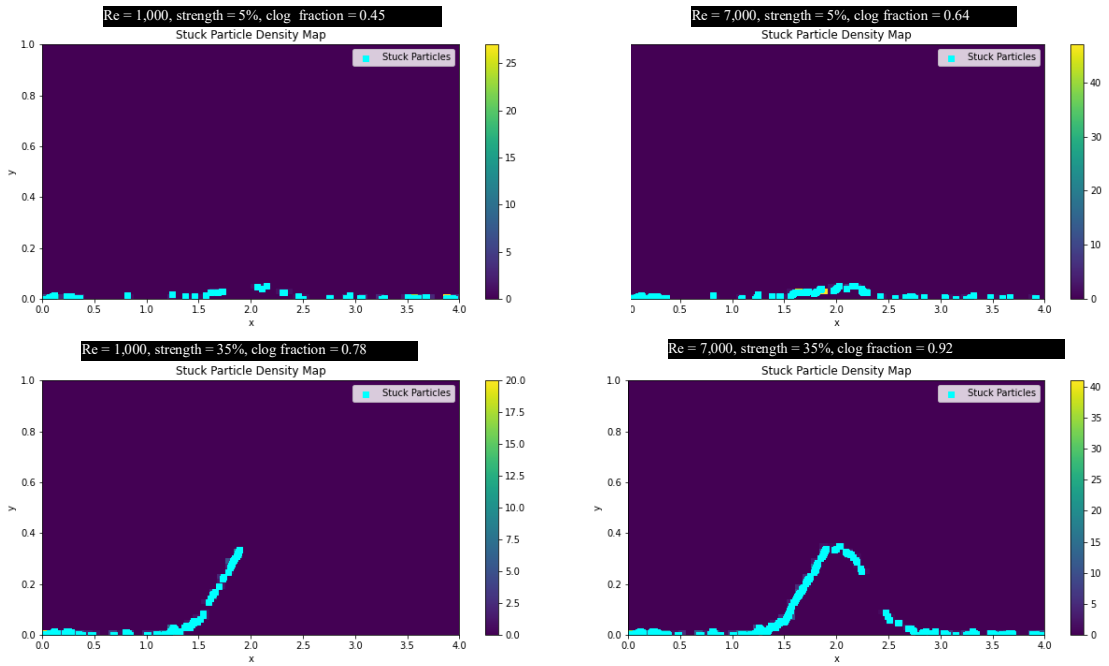

Figure 8: Density Map of Particle Deposition of Gaussian Constriction for Different Strength and Re

3. Discussion

I used numerical simulations to study the dynamics of incompressible fluid flow in channels in a direct and visual manner. At different Reynolds numbers, my solutions successfully reproduced the parabolic velocity profile described by Poiseuille's law, and the simulations agreed closely with the theoretical analytical solution. To better mimic realistic scenarios, I introduced rough channel walls and localized constrictions. In these cases, I observed that the fluid accelerated through the narrow regions, forming jet-like flows and recirculation zones. This effect was particularly pronounced at higher Reynolds numbers, where inertial forces dominate over viscous dissipation.

To quantify the impact of constriction severity and Reynolds number, I calculated the flow resistance, Strouhal number, and energy dissipation. The results showed that both resistance and energy dissipation increased with stronger constrictions and higher Reynolds numbers. The Strouhal number remained nearly constant at mild constrictions but rose with Reynolds number when the constrictions became severe. Step-like constrictions were found to hinder flow more strongly than Gaussian-shaped ones of equal strength, leading to more intense vortex shedding and greater energy losses. This observation is physically consistent: a sharp-edged constriction produces stronger flow separation and larger shear layers, which shed vortices more violently than smoother Gaussian constrictions, where the flow can adjust more gradually. Due to computational limits, the resolution of my simulations was

relatively modest, and the simulation times were capped at 100 seconds. With greater computational power in the future, I expect to obtain higher-fidelity results and further insights.

I also introduced particles into the flow to investigate transport and deposition patterns under varying constriction geometries and Reynolds numbers, with relevance to phenomena such as arterial blockage or sediment deposition in pipelines. At low Reynolds numbers, I observed inertial focusing, a phenomenon where particles migrate to stable equilibrium positions within the cross-section rather than depositing on the walls. This effect has been observed experimentally in microfluidic channels, blood flow in capillaries, and industrial particle separation systems. At higher Reynolds numbers, deposition increased and became more uniformly distributed along the channel walls. Under strong constrictions, particles accumulated primarily upstream of the narrowing due to the recirculation zones. At even higher Reynolds numbers, turbulence enhanced particle deposition both upstream and downstream of the constriction, producing a broader and more uniform distribution.

All of these studies were carried out in two dimensions. The potential future work can extend the simulations to three dimensions to provide a more realistic picture and capture additional physical mechanisms. Overall, my work not only demonstrates the power of the Navier–Stokes equations in describing the physical essense of fluid dynamics but also provides useful clues for understanding particle transport and deposition in blood vessels and pipelines, with potential engineering and biomedical applications.

4. Methods

I numerically solved the above 2D Navier-Stokes equations with no-slip boundary conditions on the walls. A fractional step scheme (Chorin projection) was employed for time evolution[14]. The numerical simulation used finite difference method to discretize the equation on a 2D rectangular grid with spacing $dx = L_x/n_x, dy = L_y/n_y$, where n_x, n_y were number of grid points. On each grid point (x_i, y_j) where $x_i = i \cdot dx, y_j = j \cdot dy$, I stored the field (u, v, ψ, ω) where u, v were velocity along x and y axis respectively. The channel boundaries were defined with optional constrictions of different shapes (Gaussian, step, or triangular) and random roughness. The fluid flow simulation started from rest, i.e. u_x and u_y were initialized to zero. The Reynolds number $Re = \frac{GL_y^3}{16\nu^2}$ and the theoretical Poiseuille velocity at the center of the channel was $U_{Poiseuille} = \frac{GL_y^2}{8\nu}$

The simulation time was advanced using time step Δt that was subject to two stability conditions[15]:

i) CFL condition: $\Delta t_{CFL} = \frac{\min(dx,dy)}{c_{CFL} \cdot \max(|u_x|,|u_y|)}$, where $c_{CFL} = 5$ in the channel flow case

ii) Viscous stability: $\Delta t_{visc} = \frac{\min(dx,dy)^2}{c_v \cdot \nu}$, where $c_v = 4$ in the channel flow case

$\Delta t = \min(\Delta t_{CFL}, \Delta t_{visc})$ is used in the simulation

To handle the nonlinear convective term $(u \cdot \nabla)u$ stably, especially at high Reynolds numbers, a semi-Lagrangian scheme was used. For each grid point (x_i, y_j), the departure point was computed as:

$$x_b = x_i - \Delta t \cdot u_{x_{i,j}}^n, \qquad y_b = y_j - \Delta t \cdot u_{y_{i,j}}^n$$

The velocity fields u_x, u_y at x_b, y_b were interpolated using bilinear interpolation. The advective velocities were $u_{x,adv} = interp(u_x^n, x_b, y_b)$ and $u_{y,adv} = interp(u_y^n, x_b, y_b)$ using the python interpolator scipy.interpolate.interpn.

The velocity component was advanced explicitly after accounting for the viscous term $\nu\nabla^2 u$ as follows:

$$u_{x,diff,i,j} = u_{x,adv,i,j} + \Delta t \cdot \nu\nabla^2 u_{x,adv,i,j}, \qquad u_{y,diff,i,j} = u_{y,adv,i,j} + \Delta t \cdot \nu\nabla^2 u_{y,adv,i,j}$$

where the subscript "diff" stood for "diffusion" and the Laplacian operator was discretized as:

$$\nabla^2 f_{i,j} = \frac{f_{i+1,j} - 2f_{i,j} + f_{i-1,j}}{dx^2} + \frac{f_{i,j+1} - 2f_{i,j} + f_{i,j-1}}{dy^2}$$

The predicted velocity was obtained by incorporating the driving force. u_x^*, u_y^* at the wall were set to zero for no-slip conditions

$$u_{x,i,j}^* = u_{x,diff,i,j} + \Delta t \cdot G, \;\; u_{y,i,j}^* = u_{y,diff,i,j}$$

The divergence of the predicted velocity was computed using central differences:

$$\begin{aligned}(\nabla \cdot u^*)_{i,j} &= \left.\frac{\partial u_x^*}{\partial x}\right|_{i,j} + \left.\frac{\partial y_x^*}{\partial y}\right|_{i,j} \\ &= \frac{u_{x,i+1,j}^* - u_{x,i-1,j}^*}{2dx} + \frac{u_{y,i,j+1}^* - u_{x,i,j-1}^*}{2dy}\end{aligned}$$

The Poisson equation was solved for the pressure correction $\nabla^2\phi = \frac{\nabla \cdot u^*}{\Delta t}$ with homogeneous Neumann boundary conditions, i.e. $\frac{\partial \phi}{\partial n} = 0$ on the walls. It could be effectively solved by SciPy's banded solver. Finally the velocity was corrected to satisfy incompressibility condition using:

$$u_{x,i+1,j}^{n+1} = u_{x,i,j}^* - \Delta t \cdot \left.\frac{\partial \phi}{\partial x}\right|_{i,j}, \qquad u_{y,i+1,j}^{n+1} = u_{y,i,j}^* - \Delta t \cdot \left.\frac{\partial \phi}{\partial y}\right|_{i,j}$$

The energy dissipation rate measures the irreversible conversion of kinetic energy into heat due to viscous effects. For incompressible Newtonian fluids, the local dissipation rate per unit volume is given by:

$$\Phi = 2\nu S_{ij} S_{ij}$$

where S_{ij} is the symmetric strain rate tensor $S_{ij} = \frac{1}{2}(\frac{\partial u_i}{\partial x_j} + \frac{\partial u_j}{\partial x_i})$, and repeated indices imply summation (Einstein notation). In 2D Cartesian coordinates $(i, j = x, y)$:

$$S_{xx} = \frac{\partial u_x}{\partial x}, S_{yy} = \frac{\partial u_y}{\partial y}, S_{xy} = S_{yx} = \frac{1}{2}(\frac{\partial u_x}{\partial y} + \frac{\partial u_y}{\partial x})$$

Thus,

$$\Phi = 2\nu(S_{xx}^2 + S_{yy}^2 + 2S_{xy}^2) = 2\nu\left[\left(\frac{\partial u_x}{\partial x}\right)^2 + \left(\frac{\partial u_y}{\partial y}\right)^2 + \frac{1}{2}\left(\frac{\partial u_x}{\partial y} + \frac{\partial u_y}{\partial x}\right)^2\right]$$

The total dissipation rate ϵ over the domain is the volume integral: $\epsilon = \int \Phi \, dV$.

The numerical simulation is implemented in Python and is available:
https://github.com/JH162/NavierStokes2DSimulation

5. References

1. Clay Mathematics Institute. Navier-Stokes Equation. http://www.claymath.org/millennium-problems/navier-stokes-equation (2000).
2. C.L.M.H. Navier. Mémoire sur les lois du mouvement des fluides. *Mémoires de l'Académie Royale des Sciences de l'Institut de France* **5**, 389–440 (1822).
3. G.G. Stokes. On the theories of the internal friction of fluids in motion, and of the equilibrium and motion of elastic solids. *Transactions of the Cambridge Philosophical Society* **8**, 287–305 (1845).
4. P. A. Davidson. Turbulence: An Introduction for Scientists and Engineers. Oxford University Press (2015).
5. J.L.M. Poiseuille. Recherches expérimentales sur le mouvement des liquides dans les tubes de très petits diamètres. *Comptes Rendus* **19**, 1164–1171 (1844).
6. F. M. White. Fluid Mechanics. McGraw-Hill Education (2011).
7. J. P. Matas, J. F. Morris, É. Guazzelli. Inertial migration of rigid spherical particles in Poiseuille flow. *Journal of Fluid Mechanics* **515**, 171–195 (2004).
8. D. Di Carlo. Inertial microfluidics. *Lab on a Chip* **9(21)**, 3038–3046 (2009).
9. G. Segre, A. Silberberg. Radial particle displacements in Poiseuille flow of suspensions. *Nature* **189**, 209–210 (1961).
10. D. Di Carlo, D. Irimia, R. G. Tompkins, M. Toner. Continuous inertial focusing, ordering, and separation of particles in microchannels. *Proceedings of the National Academy of Sciences* **104(48),** 18892–18897 (2007).
11. J. P. Matas, V. Glezer, É. Guazzelli, J. F. Morris. Trains of particles in finite-Reynolds-number pipe flow. *Physics of Fluids* **16(11),** 4192–4195 (2004).
12. M. R. Sippola, W. W. Nazaroff. Modeling particle loss in ventilation ducts. *Atmospheric Environment* **38(36),** 6113–6122 (2004).
13. C. Marchioli, M. V. Salvetti, A. Soldati. Some issues concerning large-eddy simulation of inertial particle dispersion in turbulent bounded flows. *Physics of Fluids* **20(4),** 040603 (2008).
14. A. J. Chorin. Numerical solution of the Navier-Stokes equations. *Mathematics of Computation* **22**(104), 745–762 (1968).
15. LeVeque, R. J., Finite Difference Methods for Ordinary and Partial Differential Equations: Steady-State and Time-Dependent Problems. *Society for Industrial and Applied Mathematics* (2007).